

INVESTIGATING THE EFFECTS OF CORE-SHELL PARTICLES ON NON-ISOTHERMAL REACTIVE LIQUID CHROMATOGRAPHY

U. D. UCHE,¹ M. UCHE, F. M. OKAFOR

ABSTRACT In this work, a two-dimensional general rate model of reactive liquid chromatography is extended to incorporate the effects of core-shell particles in non-isothermal operating conditions. The aim is to determine whether better conversion and separation of chemical components can be achieved by applying core-shell particles while operating under non-isothermal conditions when compared with fully porous particles. The model equations are derived for pulse injections into a chromatographic column of cylindrical geometry. The model equations form a nonlinear system of convection-diffusion-reaction partial differential equations coupled with algebraic equations for isotherms and reactions. A semi-discrete high resolution finite volume scheme is implemented to approximate the solutions of the system of partial differential equations. A few consistency checks are carried out to verify the model and numerical scheme accuracy. The obtained results show that although they offer shorter retention times and sharper profiles, the use of core-shell particles in reactive chromatography operations does not offer better separation of the components.

Keywords and phrases: Liquid chromatography, non-isothermal, core-shell particles, high-resolution finite volume scheme
2010 Mathematical Subject Classification: 35K57, 65M08, 76M12, 76V05, 80A20, 80A30, 80A32

1. Introduction

Liquid chromatography is a very useful technique used to separate components of complex chemical formations in laboratories and industries. The technique is a vital element of separation science and is regarded as a powerful purification and separation technique used in medicine, petrochemical, pharmaceutical, fine chemical, as well

Received by the editors October 21, 2020; Revised: July 02, 2021; Accepted: July 29, 2021

www.nigerianmathematicalsociety.org; Journal available online at <https://ojs.ictp.it/jnms/>

¹Corresponding author

as in food and bio-technical industries for refinement and subsequent analysis [1, 2, 3]. It has been used for the separation of chiral molecules, sugar, enzymes, and for the purification of proteins or insulin production [1, 2].

Various types of particles and particle sizes have been developed and applied in liquid chromatography processes successfully [4, 5, 6, 7, 8, 9, 10, 11]. These particles are manufactured in various forms which include fully porous, nonporous and core-shell particles. [5, 6, 7] showed nonporous particles to be successful in analytical liquid chromatography because they provided fast separation times. This however reduces the retention time and selectivity which causes poor peak resolution due to present low surface area. On the other hand, application of fully porous particles reduces the column efficiency due to its intraparticle mass transfer limitations. These particles can offer large binding capacities with only moderate intraparticle mass transfer resistances [11].

The use of core-shell particles (termed as superficially porous by [4], fused-core by [9] and cored beads by [10]) have been shown to provide optimum conditions by avoiding the shortcomings of both fully porous and nonporous particles. The core-shell particles used in liquid chromatography are a class of particles that are made up of a solid inert core and a porous shell. The core radius fraction is obtained as the ratio of the radius of the solid inert core to the radius of the particle (c.f. Fig. 1). The core particle size, thickness of the shell and level of porosity in the shell are designed to suit different types of chromatographic applications. [12] showed that the core-shell particle size and the porous layer thickness, influence the parameters of separation greatly. A decrease in the porous layer thickness results in an improved column efficiency and faster elution, while a larger sized core-shell particle minimizes the back pressure [13, 14].

The combination of chromatographic separation and chemical reactions under non-isothermal conditions in a single-unit operation, can lead to the production of high quality products [15]. This means that chemical reaction and separation of the chemical components are occurring at the same time as the temperature changes inside the chromatography column. This process is known as a non-isothermal reactive chromatographic process. The type of reaction, together with the desired order of components elution, largely influence the reactive chromatographic process. The situation in which

reactant elutes in the middle of the products, provides a high purity separation of products. The weakest adsorbed product can be collected outside the column with high purity when the reactant is the strongest adsorbed component, while the intermediate eluting component is obtained along with the reactant [16].

In this work, a nonlinear chromatography with reversible reactions of the type $A \rightleftharpoons B + C$, has been considered. Here, the reactant A is injected as a rectangular pulse into the chromatographic column. With the presence of the catalyst inside the column, the reactant A reacts and produces products B and C. This process is also expressed as conversion of component A to produce products B and C. For a sufficiently long elution time of reactant A inside the column, a complete conversion of component A and production and separation of products B and C can be achieved. In order to accomplish a high purity separation, the backward reaction driving force has to be suppressed by the forward reaction [3].

The application of mathematical modeling in representing the complex nature of liquid chromatographic process without carrying out extensive experiments has been shown to be very useful. There are several one-dimensional (1D) and two-dimensional (2D) mathematical models, considering different levels of complexities used to describe the mass transfer and partitioning in chromatographic processes, which exist in the literature [1, 2, 17, 18, 19, 20]. This work extends the work carried out recently in [21] considering fully porous particles for a two-dimensional general rate model (2D-GRM) of reactive liquid chromatography operated under non-isothermal conditions, to incorporate the use of core-shell particles.

In the previous work, it was determined that the conversion and separation of mixture components for columns packed with fully porous particles are better achieved under non-isothermal operating conditions for reactive chromatography. Core-shell particles have been shown to achieve better separation and column performance in multi-component mixture of non-reactive liquid chromatography for both 1D and 2D models, see [11, 22] and the references there in. Here, we investigate the application and performance of core-shell particles in conversion and separation of components in reactive non-isothermal liquid chromatography. The goal is to determine whether conversion rate of reactants and separation of components are better achieved with columns packed with core-shell or fully porous particles, when operated under non-isothermal conditions. The same second-order semi-discrete finite volume scheme used in

[21], is extended and applied to obtain approximate solutions of the equations of the model. Case studies of chemical reactions involving the suggested three-component mixtures above are given to show the coupling of thermal waves and concentration fronts.

2. THE GOVERNING EQUATIONS

In non-isothermal liquid chromatography, the transport of multi-component concentration bands is a particular case of the convection-diffusion-reaction processes. Such phenomena can be modeled mathematically by using partial differential equations, obtained by writing the mass and energy balances in a chromatographic column slice. The column is assumed to be thermally insulated and homogeneously packed, with a constant volumetric flow rate and heterogeneous reaction taking place in the solid phase. Moreover, mass and energy transfer between the stationary and mobile phases, axial and radial dispersions, and intraparticle pore diffusion are incorporated in the following mass and energy balance equations.

Let t denote the time coordinate, z represent the axial coordinate along the column length, and r denote the radial coordinate along the column radius of a cylindrical geometry. Both the reactant and products travel along the column axis in the z -direction by convection and axial dispersion, spreads along the column radius in the r -direction by radial dispersion and the reactant decays and produces the products due to chemical reactions in the solid phase. The solute is considered to be injected in the same process described in [21], which leads to three possible ways of injection; via an inner core region, an outer core and through the whole cross-section of the cylindrical column. Thus, the mass balance equations is given for $i = 1, 2, \dots, N_c$ as

$$\begin{aligned} \frac{\partial c_{b,i}}{\partial t} + u \frac{\partial c_{b,i}}{\partial z} &= D_{z,i} \frac{\partial^2 c_{b,i}}{\partial z^2} + D_{r,i} \left(\frac{\partial^2 c_{b,i}}{\partial r^2} + \frac{1}{r} \frac{\partial c_{b,i}}{\partial r} \right) \\ &\quad - \frac{3}{R_p} F_b k_{\text{ext},i} (c_{b,i} - c_{p,i}(r_p = R_p)), \end{aligned} \quad (1)$$

where $c_{b,i}$ is the concentration of i th component in the bulk phase, $c_{p,i}$ denotes the same component concentration in the pores of the particle, u denotes the velocity, $D_{z,i}$ denotes the dispersion coefficient of the i th component in the axial direction, the phase ratio is denoted by $F_b = (1 - \epsilon_b)/\epsilon_b$, where ϵ_b denotes the external porosity, $D_{r,i}$ denotes the dispersion coefficient of the i th component in the radial direction and $k_{\text{ext},i}$ denotes the coefficient of external mass

transfer. Lastly, r_p is the radial coordinate of spherical particles of radius R_p and N_c stands for the number components in the mixture.

The corresponding equation of mass for the solute in the particles pores can be given as

$$\begin{aligned} \frac{\partial c_{p,i}}{\partial t} + F_p \frac{\partial q_{p,i}}{\partial t} = D_{p,i} \left(\frac{\partial^2 c_{p,i}}{\partial r_p^2} + \frac{2}{r_p} \frac{\partial c_{p,i}}{\partial r_p} \right) \\ + F_p \nu_i r^{\text{het}}, \quad i = 1, 2, \dots, N_c, \end{aligned} \quad (2)$$

where $q_{p,i}$ is the solid phase concentration at local equilibrium for i th component, $D_{p,i}$ is the pore diffusivity for the i th component, $F_p = \frac{1-\epsilon_p}{\epsilon_p}$, where ϵ_p is the internal porosity, ν_i are the corresponding stoichiometric coefficients of components, and r^{het} denotes the heterogeneous reaction rate in the solid phase.

Due to the non-isothermal nature of the column, the corresponding energy balance of the column, assuming also heat conductivity in the radial direction of the column, is given as

$$\begin{aligned} \frac{\partial T_b}{\partial t} + u \frac{\partial T_b}{\partial z} = \frac{\lambda_{\text{eff},z}}{\epsilon_b \rho^L c_p^L} \frac{\partial^2 T_b}{\partial z^2} + \frac{\lambda_{\text{eff},r}}{\epsilon_b \rho^L c_p^L} \left(\frac{\partial^2 T_b}{\partial r^2} + \frac{1}{r} \frac{\partial T_b}{\partial r} \right) \\ - \frac{3F_b}{R_p \rho^L c_p^L} h_{\text{eff}} (T_b - T_p(r_p = R_p)), \end{aligned} \quad (3)$$

where, T_b and T_p are respectively temperatures of the bulk fluid and fluid inside the particles pores, $\lambda_{\text{eff},z}$ represents the effective axial heat conductivity, $\lambda_{\text{eff},r}$ denotes the effective radial heat conductivity, and h_{eff} is the effective particle to fluid heat transfer coefficient.

An energy balance law for the radial temperature profile inside particles pores is expressed as

$$\begin{aligned} \left(1 + F_p \frac{\rho^S c_p^S}{\rho^L c_p^L} \right) \frac{\partial T_p}{\partial t} - F_p \sum_{j=1}^{N_c} \frac{(-\Delta H_{A,j})}{\rho^L c_p^L} \frac{\partial q_{p,i}}{\partial t} = \frac{\lambda_p}{\rho^L c_p^L} \left(\frac{\partial^2 T_p}{\partial r_p^2} + \frac{2}{r_p} \frac{\partial T_p}{\partial r_p} \right) \\ + F_p \frac{(-\Delta H_R)}{\rho^L c_p^L} r^{\text{het}}. \end{aligned} \quad (4)$$

Here, λ_p denotes the internal heat diffusivity coefficient, ρ^L and ρ^S are the densities of liquid and solid phases and c_p^L and c_p^S are the corresponding heat capacities. The ρ^L , ρ^S , c_p^L and c_p^S are considered independent of temperature, which is valid in a small range of temperature. Furthermore, $\Delta H_{A,i}$ is the enthalpy of adsorption of i th component and ΔH_R denotes the enthalpy of reaction. The

nonlinear adsorption isotherm is given as

$$q_{p,i} = \frac{a_i^{\text{ref}} c_{p,i} \exp\left(\frac{-\Delta H_{A,i}}{R_g} \left(\frac{1}{T_p} - \frac{1}{T^{\text{ref}}}\right)\right)}{1 + \sum_{j=1}^{N_c} b_j^{\text{ref}} \exp\left(\frac{-\Delta H_{A,j}}{R_g} \left(\frac{1}{T_p} - \frac{1}{T^{\text{ref}}}\right)\right) c_{p,j}}, \quad (5)$$

where a_i^{ref} and b_i^{ref} are the Henry's constant and nonlinearity coefficient of the i th component at reference temperature respectively, R_g is the gas constant, and T_{ref} represents the reference temperature.

The chemical reactions inside a chromatographic reactor can be catalyzed homogeneously (occurring in the liquid phase), heterogeneously (occurring in the solid phase) or both homogeneously and heterogeneously. In this study, only the heterogeneous (solid phase) reaction is considered. The reaction rate for a three-component model reaction ($A \rightleftharpoons B + C$) is given as

$$r^{\text{het}} = k^{\text{het}}(T_p) \left(q_{p,A} - \frac{q_{p,B} q_{p,C}}{K_{eq}^{\text{het}}} \right). \quad (6)$$

Here, k^{het} and K_{eq}^{het} respectively represent the forward heterogeneous rate of reaction constant and reaction equilibrium constant. The Arrhenius equation is used to characterize the temperature effects on the chemical reaction rates using the activation energies E_A^{het} :

$$k^{\text{het}}(T_p) = k^{\text{het}}(T^{\text{ref}}) \exp\left(\frac{-E_A^{\text{het}}}{R_g} \left(\frac{1}{T_p} - \frac{1}{T^{\text{ref}}}\right)\right). \quad (7)$$

Next, the following dimensionless variables are introduced for a reduction of the equations parameters

$$\tau = \frac{ut}{L}, \quad x = \frac{z}{L}, \quad \rho_p = \frac{r_p}{R_p}, \quad \rho = \frac{r}{R_c}, \quad Pe_{z,i} = \frac{Lu}{D_{z,i}}, \quad Pe_{z,T} = \frac{\epsilon_b Lu \rho^L c_p^L}{\lambda_{\text{eff},z}}, \quad (8a)$$

$$Pe_{\rho,T} = \frac{\epsilon_b R_c^2 u \rho^L c_p^L}{\lambda_{\text{eff},r} L}, \quad Pe_{\rho,i} = \frac{R_c^2 u}{D_{r,i} L}, \quad \zeta_i = \frac{k_{\text{ext}} R_p}{D_{p,i}}, \quad \zeta_T = \frac{h_{\text{eff}} R_p}{\lambda_p}, \quad (8b)$$

$$\eta_i = \frac{D_{p,i} L}{R_p^2 u}, \quad \eta_T = \frac{\lambda_p L}{R_p^2 u \rho^L c_p^L}, \quad \xi_i = 3\zeta_i \eta_i F_b, \quad \xi_T = 3\zeta_T \eta_T F_b, \quad (8c)$$

where L denotes the column length, $Pe_{z,i}$ and $Pe_{z,T}$ are the axial Peclet numbers, $Pe_{\rho,i}$ and $Pe_{\rho,T}$ are the radial Peclet numbers, and ζ_i and ζ_T are Biot numbers for mass and energy, respectively. Further, η_i , η_T , ξ_i , and ξ_T are the dimensionless constants. After using the above dimensionless parameters in the mass and energy balances (c.f. Eqs. (1)-(4)), the following equations are obtained for

$i = 1, 2, \dots, N_c$:

$$\frac{\partial c_{b,i}}{\partial \tau} + \frac{\partial c_{b,i}}{\partial x} = \frac{1}{Pe_{z,i}} \frac{\partial^2 c_{b,i}}{\partial x^2} + \frac{1}{Pe_{\rho,i}} \left(\frac{\partial^2 c_{b,i}}{\partial \rho^2} + \frac{1}{\rho} \frac{\partial c_{b,i}}{\partial \rho} \right) - \xi_i [c_{b,i} - c_{p,i}(\rho_p = 1)], \quad (9)$$

$$\frac{\partial c_{p,i}}{\partial \tau} + F_p \frac{\partial q_{p,i}}{\partial \tau} = \eta_i \left(\frac{\partial^2 c_{p,i}}{\partial \rho_p^2} + \frac{2}{\rho_p} \frac{\partial c_{p,i}}{\partial \rho_p} \right) + F_p \frac{L}{u} \nu_i r^{\text{het}}, \quad (10)$$

$$\frac{\partial T_b}{\partial \tau} + \frac{\partial T_b}{\partial x} = \frac{1}{Pe_{z,T}} \frac{\partial^2 T_b}{\partial x^2} + \frac{1}{Pe_{\rho,T}} \left(\frac{\partial^2 T_b}{\partial \rho^2} + \frac{1}{\rho} \frac{\partial T_b}{\partial \rho} \right) - \xi_T [T_b - T_p(\rho_p = 1)], \quad (11)$$

$$\left(1 + F_p \frac{\rho^S c_p^S}{\rho^L c_p^L} \right) \frac{\partial T_p}{\partial \tau} - F_p \sum_{j=1}^{N_c} \frac{(-\Delta H_{A,j})}{\rho^L c_p^L} \frac{\partial q_{p,i}}{\partial \tau} = \eta_T \left(\frac{\partial^2 T_p}{\partial \rho_p^2} + \frac{2}{\rho_p} \frac{\partial T_p}{\partial \rho_p} \right) + F_p \frac{(-\Delta H_R) L}{\rho^L c_p^L} \frac{r^{\text{het}}}{u}. \quad (12)$$

Recently, the case where the chromatographic column is packed with fully porous particles was investigated, see [21]. Here, in order to study the effects of core-shell particles for non-isothermal operating condition, the same procedures as described in [10] and [22] are applied. Figure 1 describes a core-shell particle for arbitrary core radius fraction $\rho_{\text{core}} = R_{\text{core}}/R_p$. Hence, in Eqs. (10) and (12),

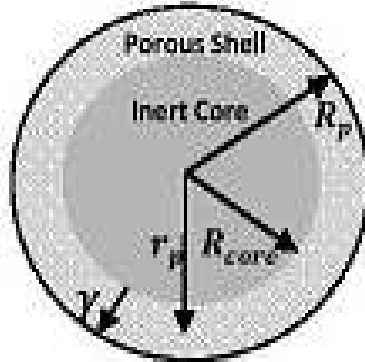


FIGURE 1. Schematic diagram of a core-shell particle.

$0 \leq \rho_p \leq 1$ for fully porous particles, and $\rho_{\text{core}} \leq \rho_p \leq 1$ for core-shell particles. This implies that $\rho_{\text{core}} = 0$ for fully porous particles and $\rho_{\text{core}} \neq 0$ for core-shell particles. Therefore, the ρ_p -axis is replaced by a new axis $0 \leq \gamma \leq 1$, given in its dimensionless form

as

$$\gamma = \frac{\rho_p - \rho_{\text{core}}}{1 - \rho_{\text{core}}}. \quad (13)$$

From Eq. (13), the following expression is obtained

$$\rho_p = \gamma(1 - \rho_{\text{core}}) + \rho_{\text{core}} \quad (14)$$

and substituted in Eqs. (10) and (12) to obtain the mass and energy balance equations for columns packed with core-shell particles, for $i = 1, 2, \dots, N_c$

$$\frac{\partial c_{b,i}}{\partial \tau} + \frac{\partial c_{b,i}}{\partial x} = \frac{1}{Pe_{z,i}} \frac{\partial^2 c_{b,i}}{\partial x^2} + \frac{1}{Pe_{\rho,i}} \left(\frac{\partial^2 c_{b,i}}{\partial \rho^2} + \frac{1}{\rho} \frac{\partial c_{b,i}}{\partial \rho} \right) - \xi_i (c_{b,i} - c_{p,i}|_{\gamma=1}), \quad (15)$$

$$\begin{aligned} & \frac{\partial c_{p,i}}{\partial \tau} + F_p \frac{\partial q_{p,i}}{\partial \tau} \\ &= \eta_i \left[\frac{1}{(1 - \rho_{\text{core}})^2} \frac{\partial^2 c_{p,i}}{\partial \gamma^2} + \frac{2}{\gamma(1 - \rho_{\text{core}})^2 + \rho_{\text{core}}(1 - \rho_{\text{core}})} \frac{\partial c_{p,i}}{\partial \gamma} \right] + F_p \frac{L}{u} \nu_i r^{\text{het}}, \end{aligned} \quad (16)$$

$$\frac{\partial T_b}{\partial \tau} + \frac{\partial T_b}{\partial x} = \frac{1}{Pe_{z,T}} \frac{\partial^2 T_b}{\partial x^2} + \frac{1}{Pe_{\rho,T}} \left(\frac{\partial^2 T_b}{\partial \rho^2} + \frac{1}{\rho} \frac{\partial T_b}{\partial \rho} \right) - \xi_T [T_b - T_p|_{\gamma=1}], \quad (17)$$

$$\begin{aligned} & \alpha^* \frac{\partial T_p}{\partial \tau} + F_p \frac{\sum_{j=1}^{N_c} (\Delta H_{A,j})}{\rho^L c_p^L} \frac{\partial q_{p,i}}{\partial \tau} \\ &= \eta_T \left[\frac{1}{(1 - \rho_{\text{core}})^2} \frac{\partial^2 T_p}{\partial \gamma^2} + \frac{2}{\gamma(1 - \rho_{\text{core}})^2 + \rho_{\text{core}}(1 - \rho_{\text{core}})} \frac{\partial T_p}{\partial \gamma} \right] + F_p \frac{\vartheta L}{u} r^{\text{het}}, \end{aligned} \quad (18)$$

where $\alpha^* = \left(1 + F_p \frac{\rho_p^S c_p^S}{\rho^L c_p^L}\right)$ and $\vartheta = \frac{(-\Delta H_R)}{\rho^L c_p^L}$.

To proceed, the following initial and boundary conditions are described. The initial conditions are given as

$$c_{b,i}(\rho, x, 0) = 0, \quad T_b(\rho, x, 0) = T_b^{\text{init}}, \quad 0 \leq x \leq 1, \quad 0 \leq \rho \leq 1, \quad (19)$$

$$c_{p,i}(\gamma, \rho, x, 0) = 0, \quad T_p(\gamma, \rho, x, 0) = T_p^{\text{init}}, \quad 0 \leq x \leq 1, \quad 0 \leq \rho \leq 1, \quad 0 \leq \gamma \leq 1, \quad (20)$$

where T_b^{init} and T_p^{init} represent the initial bulk and particle temperatures. The following boundary conditions are considered for Eqs. (15) and (17) at $\rho = 0$ and $\rho = 1$:

$$\frac{\partial c_{b,i}(\rho = 0, x, \tau)}{\partial \rho} = 0, \quad \frac{\partial c_{b,i}(\rho = 1, x, \tau)}{\partial \rho} = 0, \quad (21)$$

$$\frac{\partial T_b(\rho = 0, x, \tau)}{\partial \rho} = 0, \quad \frac{\partial T_b(\rho = 1, x, \tau)}{\partial \rho} = 0. \quad (22)$$

Also, for Eqs. (15) and (17), the following Danckwerts boundary conditions are used for injections via the inner region:

$$c_{b,i}(\rho, x = 0, \tau) - \frac{1}{Pe_{z,i}} \frac{\partial c_{b,i}(\rho, x = 0, \tau)}{\partial x} = \begin{cases} c_{b,i}^{\text{inj}}, & \text{if } 0 \leq \rho \leq \tilde{\rho} \text{ and } 0 \leq \tau \leq \tau_{\text{inj}}, \\ 0, & \tilde{\rho} < \rho \leq 1 \text{ or } \tau > \tau_{\text{inj}}, \end{cases} \quad (23a)$$

$$T_b(\rho, x=0, \tau) - \frac{1}{Pe_{z,T}} \frac{\partial T_b(\rho, x=0, \tau)}{\partial x} = \begin{cases} T_b^{\text{inj}}, & \text{if } 0 \leq \rho \leq \tilde{\rho} \text{ and } 0 \leq \tau \leq \tau_{\text{inj}}, \\ 0, & \tilde{\rho} < \rho \leq 1 \text{ or } \tau > \tau_{\text{inj}}. \end{cases} \quad (23b)$$

Here, the symbols $c_{b,i}^{\text{inj}}$ and T_b^{inj} are used to denote the inlet concentration of component i and the bulk temperature. In this work, T_b^{inj} , T_b^{init} and T^{ref} are taken to be identical. At the column outlet ($x = 1$), the zero Neumann boundary conditions are utilized:

$$\frac{\partial c_{b,i}}{\partial x} = 0, \quad \frac{\partial T_b}{\partial x} = 0. \quad (23c)$$

For Eqs. (16) and (18), the boundary conditions at $\gamma = 0$ and $\gamma = 1$ are given as

$$\left. \frac{\partial c_{p,i}}{\partial \gamma} \right|_{\gamma=0} = 0, \quad \left. \frac{\partial c_{p,i}}{\partial \gamma} \right|_{\gamma=1} = (1 - \rho_{\text{core}}) \zeta_i(c_{b,i} - c_{p,i}|_{\gamma=1}), \quad (23d)$$

$$\left. \frac{\partial T_p}{\partial \gamma} \right|_{\gamma=0} = 0, \quad \left. \frac{\partial T_p}{\partial \gamma} \right|_{\gamma=1} = (1 - \rho_{\text{core}}) \zeta_T(T_b - T_p|_{\gamma=1}). \quad (23e)$$

3. NUMERICAL SCHEME IMPLEMENTATION

Numerical schemes are important to obtain approximate solutions of nonlinear equations, such as the ones governing the above described model. There are several numerical schemes that can be used to approximate the solutions of the above model equations [18, 2, 23, 24] and the references therein. Here, the semi-discrete finite volume method used in [22], is again applied. The method has been shown to be simple, compact, easily implemented, and second order accurate [23, 25]. The order of accuracy of the suggested scheme has already been verified analytically and numerically, see (c.f. [23]). The process of formulating the numerical is described below.

The following system of equations are obtained from Eqs. (15)-(18) by using the adsorption isotherm described in Eq. (5) for a mixture of three components:

$$\frac{\partial \mathbf{c}_b}{\partial \tau} + \frac{\partial \mathbf{c}_b}{\partial x} = \mathbf{P}_z \frac{\partial^2 \mathbf{c}_b}{\partial x^2} + \mathbf{P}_\rho \left(\frac{\partial^2 \mathbf{c}_b}{\partial \rho^2} + \frac{1}{\rho} \frac{\partial \mathbf{c}_b}{\partial \rho} \right) - \xi(\mathbf{c}_b - \mathbf{c}_p(\gamma = 1)), \quad (24)$$

$$\mathbf{J} \frac{\partial \mathbf{c}_p}{\partial \tau} = \eta \left(\frac{1}{(1 - \rho_{\text{core}})^2} \frac{\partial^2 \mathbf{c}_p}{\partial \gamma^2} + \frac{2}{\gamma(1 - \rho_{\text{core}})^2 + \rho_{\text{core}}(1 - \rho_{\text{core}})} \frac{\partial \mathbf{c}_p}{\partial \gamma} \right) + F_p \frac{L}{u} \mathbf{R}r^{\text{het}}, \quad (25)$$

where

$$\begin{aligned}
\mathbf{c}_b &= \begin{bmatrix} c_{b,1} \\ c_{b,2} \\ c_{b,3} \\ T_b \end{bmatrix}, \quad \mathbf{c}_p = \begin{bmatrix} c_{p,1} \\ c_{p,2} \\ c_{p,3} \\ T_p \end{bmatrix}, \quad \mathbf{P}_z = \begin{bmatrix} \frac{1}{Pe_{z,1}} & 0 & 0 & 0 \\ 0 & \frac{1}{Pe_{z,2}} & 0 & 0 \\ 0 & 0 & \frac{1}{Pe_{z,3}} & 0 \\ 0 & 0 & 0 & \frac{1}{Pe_{z,T}} \end{bmatrix}, \\
\xi &= \begin{bmatrix} \xi_1 & 0 & 0 & 0 \\ 0 & \xi_2 & 0 & 0 \\ 0 & 0 & \xi_3 & 0 \\ 0 & 0 & 0 & \xi_T \end{bmatrix}, \quad \eta = \begin{bmatrix} \eta_1 & 0 & 0 & 0 \\ 0 & \eta_2 & 0 & 0 \\ 0 & 0 & \eta_3 & 0 \\ 0 & 0 & 0 & \eta_T \end{bmatrix}, \\
\mathbf{P}_\rho &= \begin{bmatrix} \frac{1}{Pe_{\rho,1}} & 0 & 0 & 0 \\ 0 & \frac{1}{Pe_{\rho,2}} & 0 & 0 \\ 0 & 0 & \frac{1}{Pe_{\rho,3}} & 0 \\ 0 & 0 & 0 & \frac{1}{Pe_{\rho,T}} \end{bmatrix}, \quad \mathbf{R} = \begin{bmatrix} \nu_1 & 0 & 0 & 0 \\ 0 & \nu_2 & 0 & 0 \\ 0 & 0 & \nu_3 & 0 \\ 0 & 0 & 0 & \vartheta \end{bmatrix}, \\
\mathbf{J} &= \begin{bmatrix} 1 + F_p \frac{\partial q_{p,1}}{\partial c_{p,1}} & F_p \frac{\partial q_{p,1}}{\partial c_{p,2}} & F_p \frac{\partial q_{p,1}}{\partial c_{p,3}} & F_p \frac{\partial q_{p,1}}{\partial T_p} \\ F_p \frac{\partial q_{p,2}}{\partial c_{p,1}} & 1 + F_p \frac{\partial q_{p,2}}{\partial c_{p,2}} & F_p \frac{\partial q_{p,2}}{\partial c_{p,3}} & F_p \frac{\partial q_{p,2}}{\partial T_p} \\ F_p \frac{\partial q_{p,3}}{\partial c_{p,1}} & F_p \frac{\partial q_{p,3}}{\partial c_{p,2}} & 1 + F_p \frac{\partial q_{p,3}}{\partial c_{p,3}} & F_p \frac{\partial q_{p,3}}{\partial T_p} \\ \beta^* \sum_{j=1}^3 \frac{\partial q_{p,j}}{\partial c_{p,1}} & \beta^* \sum_{j=1}^3 \frac{\partial q_{p,j}}{\partial c_{p,2}} & \beta^* \sum_{j=1}^3 \frac{\partial q_{p,j}}{\partial c_{p,3}} & \alpha^* + \beta^* \sum_{j=1}^3 \frac{\partial q_{p,j}}{\partial T_p} \end{bmatrix}, \tag{26}
\end{aligned}$$

where $\beta^* = F_p \frac{\Delta H_A}{\rho^L c_p^L}$. For the case where all the nonlinearity coefficients b_j^{ref} are zero, then the above Jacobian matrix J becomes easier to handle. In order to derive the scheme, we first discretize the domain of computations.

Discretizing the domains: A domain $[0, 1] \times [0, 1] \times [0, 1]$, enclosed by the cells $\Omega_{klm} \equiv [x_{k-\frac{1}{2}}, x_{k+\frac{1}{2}}] \times [\rho_{l-\frac{1}{2}}, \rho_{l+\frac{1}{2}}] \times [\gamma_{m-\frac{1}{2}}, \gamma_{m+\frac{1}{2}}]$ for $1 \leq k \leq N_x$, $1 \leq l \leq N_\rho$ and $1 \leq m \leq N_\gamma$, is considered. The coordinate points in the cell Ω_{klm} are represented by (x_k, ρ_l, γ_m) . Here,

$$x_k = \frac{x_{k-\frac{1}{2}} + x_{k+\frac{1}{2}}}{2}, \quad \rho_l = \frac{\rho_{l-\frac{1}{2}} + \rho_{l+\frac{1}{2}}}{2}, \quad \gamma_m = \frac{\gamma_{m-\frac{1}{2}} + \gamma_{m+\frac{1}{2}}}{2} \tag{27}$$

and for this uniform mesh

$$\Delta x = x_{k-\frac{1}{2}} - x_{k+\frac{1}{2}}, \quad \Delta \rho = \rho_{l-\frac{1}{2}} - \rho_{l+\frac{1}{2}}, \quad \Delta \gamma = \gamma_{m-\frac{1}{2}} - \gamma_{m+\frac{1}{2}}. \tag{28}$$

Note that

$$c_b := c_b(\rho, x, \tau) \quad \text{and} \quad c_p := c_p(\gamma, \rho, x, \tau). \tag{29}$$

Therefore, for $I_{kl} := [x_{k-\frac{1}{2}}, x_{k+\frac{1}{2}}] \times [\rho_{l-\frac{1}{2}}, \rho_{l+\frac{1}{2}}]$ and Ω_{klm} , the averaged values of the cell $c_{b,k,l}(\tau)$ and $c_{p,k,l,m}(\tau)$ are expressed at any time τ as

$$c_{b,k,l} = c_{b,k,l}(\tau) = \frac{1}{\Delta x_k \Delta \rho_l} \int_{I_{kl}} c_b(\rho, x, \tau) d\rho dx, \quad (30)$$

$$c_{p,k,l,m} = c_{p,k,l,m}(\tau) = \frac{1}{\Delta x_k \Delta \rho_l \Delta \gamma_m} \int_{\Omega_{klm}} c(\gamma, \rho, x, \tau) d\gamma d\rho dx. \quad (31)$$

By integrating Eq. (24) over the interval I_{kl} and using Eqs. (30) and (31), the following expression is obtained:

$$\begin{aligned} \frac{dc_{b,k,l}}{d\tau} = & - \frac{\mathbf{c}_{b,k+\frac{1}{2},l} - \mathbf{c}_{b,k-\frac{1}{2},l}}{\Delta x} + \frac{\mathbf{P}_z}{\Delta x} \left[\left(\frac{\partial \mathbf{c}_b}{\partial x} \right)_{k+\frac{1}{2},l} - \left(\frac{\partial \mathbf{c}_b}{\partial x} \right)_{k-\frac{1}{2},l} \right] \\ & + \frac{\mathbf{P}_\rho}{\Delta \rho} \left[\left(\frac{\partial \mathbf{c}_b}{\partial \rho} \right)_{k,l+\frac{1}{2}} - \left(\frac{\partial \mathbf{c}_b}{\partial \rho} \right)_{k,l-\frac{1}{2}} + \frac{\mathbf{c}_{b,k,l+\frac{1}{2}} - \mathbf{c}_{b,k,l-\frac{1}{2}}}{\rho_{l+\frac{1}{2}}} \right] \\ & - \xi (\mathbf{c}_{b,k,l} - \mathbf{c}_{p,k,l,N_\gamma}), \end{aligned} \quad (32)$$

where $k = 1, 2, \dots, N_x$ and $l = 1, 2, \dots, N_\rho$. The derivatives appearing in the above equations are approximated as

$$\left(\frac{\partial \mathbf{c}_b}{\partial x} \right)_{k \pm \frac{1}{2},l} = \pm \frac{(\mathbf{c}_{b,k \pm 1,l} - \mathbf{c}_{b,k,l})}{\Delta x}, \quad \left(\frac{\partial \mathbf{c}_b}{\partial \rho} \right)_{k,l \pm \frac{1}{2}} = \pm \frac{(\mathbf{c}_{b,k,l \pm 1} - \mathbf{c}_{b,k,l})}{\Delta \rho}. \quad (33)$$

Integration of equation (25) over the interval Ω_{ij} leads to:

$$\frac{dc_{p,k,l,m}}{d\tau} = \mathbf{J}_{k,l,m}^{-1} \frac{1}{\epsilon_p \gamma^2_{m+1/2} \Delta \gamma} [(\mathbf{c}_p)_{k,l,m+1/2} - (\mathbf{c}_p)_{k,l,m-1/2}] + F_p \frac{L}{u} \mathbf{J}_{k,l,m}^{-1} \mathbf{R}_{k,l,m}^{\text{het}}, \quad (34)$$

with the interface flux given as

$$\begin{aligned} (\mathbf{c}_p)_{k,l,m+1/2} = & \max \left(\frac{(\mathbf{c}_p)_{k,l,m+1} - (\mathbf{c}_p)_{k,l,m}}{\Delta \gamma}, 0 \right) \gamma^2_{m+1} \\ & + \min \left(\frac{(\mathbf{c}_p)_{k,l,m+1} - (\mathbf{c}_p)_{k,l,m}}{\Delta \gamma}, 0 \right) \gamma^2_m. \end{aligned} \quad (35)$$

Similarly, $(\mathbf{c}_p)_{k,l,m-1/2}$ can be defined by just lowering the index m by one in the above equation. The fluxes at the cell interfaces $x_{k \pm \frac{1}{2}}$, $\rho_{l \pm \frac{1}{2}}$ and $\gamma_{m \pm \frac{1}{2}}$ in Eqs. (32) and (34) are approximated by using the following schemes along with the total variation diminishing Runge-Kutta (TVD-RK) scheme to get a second order accuracy in time [23, 26].

First order scheme: The axial flux vectors \mathbf{c}_b and \mathbf{c}_p at the interfaces of the cell are approximated as follows

$$\mathbf{c}_{b,k,l+\frac{1}{2}} = \mathbf{c}_{b,k,l} \quad \mathbf{c}_{b,k,l-\frac{1}{2}} = \mathbf{c}_{b,k,l-1}, \quad (36)$$

$$\mathbf{c}_{p,k,l,m+\frac{1}{2}} = \mathbf{c}_{p,k,l,m} \quad \mathbf{c}_{p,k,l,m-\frac{1}{2}} = \mathbf{c}_{p,k,l,m-1}. \quad (37)$$

The approximations above, provide a first order accuracy of the scheme along the axial-coordinate.

Second order scheme: Here, the axial flux vectors are approximated by using the following expressions:

$$\begin{aligned} \mathbf{c}_{b,k,l+\frac{1}{2}} &= \mathbf{c}_{b,k,l} + \frac{1}{2}\varphi(\alpha_{k,l})(\mathbf{c}_{b,k,l} - \mathbf{c}_{b,k,l-1}), \\ \alpha_{k,l} &= \frac{\mathbf{c}_{b,k,l+1} - \mathbf{c}_{b,k,l} + \xi^*}{\mathbf{c}_{b,k,l} - \mathbf{c}_{b,k,l-1} + \xi^*}, \end{aligned} \quad (38)$$

$$\begin{aligned} \mathbf{c}_{p,k,l,m+\frac{1}{2}} &= \mathbf{c}_{p,k,l,m} + \frac{1}{2}\phi(\beta_{k,l,m})(\mathbf{c}_{p,k,l,m} - \mathbf{c}_{p,k,l,m-1}), \\ \beta_{k,l,m} &= \frac{\mathbf{c}_{p,k,l,m+1} - \mathbf{c}_{p,k,l,m} + \xi^*}{\mathbf{c}_{p,k,l,m} - \mathbf{c}_{p,k,l,m-1} + \xi^*}. \end{aligned} \quad (39)$$

Eqs. (38) and (39) produces a flux-limiting high resolution scheme. A small value of ξ^* , e.g. $\xi^* = 10^{-10}$, is selected to avoid the situation of division by zero. The local monotonicity of the scheme is preserved by utilizing the flux limiting functions φ and ϕ as defined below (c.f. [23])

$$\varphi(\alpha_{k,l}) = \max \left(0, \min \left(2\alpha_{k,l}, \min \left(\frac{1}{3} + \frac{2}{3}\alpha_{k,l}, 2 \right) \right) \right), \quad (40)$$

$$\phi(\beta_{k,l,m}) = \max \left(0, \min \left(2\beta_{k,l,m}, \min \left(\frac{1}{3} + \frac{2}{3}\beta_{k,l,m}, 2 \right) \right) \right). \quad (41)$$

It is impossible to apply the high resolution scheme up to the boundary intervals. To overcome this difficulty, the aforementioned first order approximation of fluxes is used at the interfaces of boundary cells, while the suggested second order approximation of fluxes is well applicable at the interfaces of interior cells. In the current study, the interstitial velocity u is positive. Thus, a first order approximation is taken in the left boundary cell only, while such an approximation is not needed in the right boundary cell. Further, it has been found that global accuracy of the suggested algorithm is not diminished by such first order approximations in the boundary cells [23, 25].

Lastly, to solve Eqs. (32)-(41), a second order TVD-RK scheme is applied to get the second order accuracy in time [26]. The TVD-RK scheme ensures the changes in the solution do not increase as the order is increased. The right-hand-side of Eqs. (32) and (34) are represented by $\mathcal{F}(\mathbf{c}_b, \mathbf{c}_p |_{\gamma=1})$ and $\mathcal{G}(\mathbf{c}_p)$. To update the stages of \mathbf{c}_b and \mathbf{c}_p , the following second order TVD-RK scheme is utilized [26]:

$$\mathbf{c}_b^{(1)} = \mathbf{c}_b^n + \Delta\tau\mathcal{F}(\mathbf{c}_b^n, \mathbf{c}_p^n |_{\gamma=1}), \quad \mathbf{c}_b^{n+1} = \frac{1}{2}[\mathbf{c}_b^n + \mathbf{c}_b^{(1)} + \Delta\tau\mathcal{F}(\mathbf{c}_b^{(1)}, \mathbf{c}_p^{(1)} |_{\gamma=1})], \quad (42)$$

$$\mathbf{c}_p^{(1)} = \mathbf{c}_p^n + \Delta\tau\mathcal{G}(\mathbf{c}_p^n), \quad \mathbf{c}_p^{n+1} = \frac{1}{2}[\mathbf{c}_p^n + \mathbf{c}_p^{(1)} + \Delta\tau\mathcal{G}(\mathbf{c}_p^{(1)})]. \quad (43)$$

In the above expressions, solutions at previous time-step τ^n are represented by \mathbf{c}_b^n and \mathbf{c}_p^n , while solutions at new time-step τ^{n+1} , the solutions are represented by \mathbf{c}_b^{n+1} and \mathbf{c}_p^{n+1} . A Courant-Friedrichs-Lewy (CFL) condition defined below is used to choose the time step $\Delta\tau$:

$$\Delta\tau \leq \frac{12}{\min} \left(\Delta x, \Delta x^2 \min(Pe_{z,i}, Pe_{z,T}), \frac{\Delta\gamma^2(1 - \rho_{\text{core}})^2}{2 \max(\mathbf{J}_{k,l,m}^{-1} \eta)}, \frac{\rho_{\text{core}}(1 - \rho_{\text{core}})\Delta\gamma}{\max(\mathbf{J}_{k,l,m}^{-1} \eta)} \right). \quad (44)$$

The above method was programmed in C language with a mesh size of $60 \times 30 \times 10$.

4. RESULTS CONSISTENCY VALIDATION

The integral consistency tests for mass and energy balance equations are useful tools for the validation of numerically obtained results and the accuracy of the developed model. These tests are used to evaluate the accuracy of numerical schemes and the conservation of mass and energy balances.

Given a reversible chemical reaction of the form $A \rightleftharpoons B+C$, the following expressions are utilized to validate the consistency of the results obtained from our numerical scheme [21, 27], let ξ describe a change in the number of moles due to the chemical reaction, i.e.

$$\xi = n_1^{\text{inj}} - n_1^{\text{out}} = n_2^{\text{out}} + n_3^{\text{out}}. \quad (45)$$

The total mass injected in the column is defined as

$$n_i^{\text{inj}} = c_{b,i}^{\text{inj}} V^{\text{inj}}, \quad (46)$$

where V^{inj} is the volume injected and c_b^{inj} is the concentration injected.

Furthermore, at the column outlet, we have

$$n_i^{\text{out}} = \dot{V} \int_0^{t^*} c_{b,i}(t, z = L) dt, \quad i = 1, 2, 3, \quad (47)$$

where \dot{V} is the volumetric flow rate.

Standard deviations for the three values of ξ_i are calculated as

$$\sigma_{\xi,i}[\%] = 100 \times \sqrt{\frac{\sum_{j=1}^i (\xi_j - \bar{\xi})^2}{3}}, \quad i = 1, 2, 3. \quad (48)$$

$\bar{\xi}$ represents the average of ξ_i for $i = 1, 2, 3$.

For the energy balance, we have

$$\begin{aligned} \Delta H^{\text{inj}} &= \rho^L c_p^L \dot{V} \int_0^{t^*} (T_b^{\text{inj}} - T^{\text{ref}}) dt, \\ \Delta H^{\text{out}} &= \rho^L c_p^L \dot{V} \int_0^{t^*} (T_b(t, z = L) - T^{\text{ref}}) dt, \end{aligned} \quad (49)$$

where ΔH^{inj} is the enthalpy entering and ΔH^{out} is the enthalpy leaving the system.

Lastly, a relative percentage error $E_H[\%]$ is defined as

$$E_H[\%] = 100 \times \left| \frac{\Delta H_{\text{err}}}{\Delta H_R \bar{\xi}} \right|, \quad (50)$$

where

$$\Delta H^{\text{out}} + (\Delta H_R) \bar{\xi} = \Delta H_{\text{err}}. \quad (51)$$

In the above equation (Eq. (51)), $\Delta H_{\text{err}} = 0$ only if the model equation is perfectly satisfied. However, several sources of numerical errors are involved in the computations, such as errors due to domain discretization, round off, and errors in the numerical integrations of the outlet profiles. As a result of these errors, ΔH_{err} cannot be zero. Therefore, the smaller the value of ΔH_{err} , the better is the fulfillment of the coupled mass and energy balances.

5. TEST CASES

In this section, the effects of the core radius fraction on the conversion and separation of mixture components in non-isothermal reactive liquid chromatography are analyzed. The value of the heat of adsorption for all components is taken the same, i.e. $\Delta H_{A,j} = \Delta H_A$. Furthermore, the values of the kinetic parameters $Pe_{z,i}$ and $Pe_{\rho,i}$ are also assumed the same for all the components, although in practical terms, they may vary according to components. The reactant (component 1) was injected in the inner core as a Danckwerts boundary condition for all test cases. All parameters used in these test cases are listed in Table 1, which were used by [28] and [29]

in their experimental studies for exothermic esterification reaction catalyzed by an acidic ion-exchange resin.

We begin by considering a column operating under isothermal condition for fully porous particles. In Fig. 2, the isothermal case ($\Delta H_A = 0 \text{ kJ/mol}$, $\Delta H_R = 0 \text{ kJ/mol}$) is presented for $\rho_{\text{core}} = 0$ (fully porous particles). The behavior of the concentration profiles and temperature profile is shown for the considered reversible reaction process in which only the reactant $c_{b,1}$ (component 1) is injected into the chromatographic reactor. The presence of the products $c_{b,2}$ and $c_{b,3}$ can be seen in Fig. 2(a) as a result of the values of the adsorption coefficients chosen. The temperature profile given in Fig. 2(b) shows no changes, this is true for the isothermal case being considered. In Figs. 3(a) and (b), the effects of the core radius fraction are displayed for $\rho_{\text{core}} = 0.5$ and $\rho_{\text{core}} = 0.8$ respectively. It can be seen that increasing the core radius fraction from $\rho_{\text{core}} = 0$ to $\rho_{\text{core}} = 0.8$, leads to more narrower peak and shorter retention time inside the column. But this has caused a reduction in the conversion and separation of the reactant to products, because the use of core-shell particles offer lesser binding capacities as compared with fully porous particles which provide larger binding capacities with only moderate intraparticle mass transfer resistances. The temperature profiles corresponding to Figs. 3(a) and (b) are identical to the one presented in Fig. 2(b) because of the isothermal case considered, hence they are omitted here. For these obtained results, the coefficient of nonlinearity in the suggested isotherm is taken as zero for all components, i.e. $b_j^{\text{ref}} = 0$ for $j = 1, 2, 3$. The same condition holds for other results, except the last result in which we shall consider the fully nonlinear isotherm where $b_j^{\text{ref}} = 1$ for $j = 1, 2, 3$.

Next we present the non-isothermal cases, where the results were obtained under the influence of exothermic reaction ($\Delta H_A = -60 \text{ kJ/mol}$, $\Delta H_R = -20 \text{ kJ/mol}$), beginning with Fig. 4, where the result for $\rho_{\text{core}} = 0$ is given. Again we see the appearance and behavior of the components in the concentration profiles (Fig. 4(a)) as a result of the chosen adsorption coefficients. The fluctuations in the temperature profiles can be seen in Fig. 4(b) as a result of the non-isothermal condition being considered. In Fig. 5, the result for $\rho_{\text{core}} = 0.8$ is shown. Here we see again that although the retention times of the concentration components inside the column is shorter in the case of $\rho_{\text{core}} = 0.8$ (Fig. 5(a)), better conversion and separation are achieved by fully porous particles just as was observed in the case of isothermal condition. This can also be seen

in Table 2, where the conversion rate for $\rho_{\text{core}} = 0$ is 28% and that of $\rho_{\text{core}} = 0.8$ is 14%. Other results given in Table 2 show that fully porous particles perform better in terms of separation of components for both isothermal and non-isothermal operating conditions for reactive liquid chromatography. Furthermore, the combined errors of integral energy and mass balances, expressed by the error $E_H[\%]$ (c.f. Eq. (50)) is less than 1% in all the test cases considered and, therefore, verifies the accuracy of the numerical results.

In order to show that this current 2D model fully captures the evolution of radial disturbances in the column, the three-dimensional (3D) plots of the 1D plots shown in Figs. 4 and 5, are given in Figs. 6 and 7. For the chosen value of radial Peclet number $Pe_\rho = 37.5$, which corresponds to the small radial dispersion D_r , radial variations can be easily seen on the concentration and temperature profiles. The value of the concentration is larger at the center of the column due to the injection through the inner core region, i.e. at $\rho = 0$. In Figs. 8 and 9, the effects of altering the values of the adsorption coefficients or Henry's constants, are shown. Once again, the results of the fully porous particles (Fig. 8) show a better conversion and separation. Next, Figs. 10 and 11 show the effects of the intraparticle diffusion coefficients for mass and energy (η and η_T) respectively. We see that a reduction in the values of η and η_T lead to more diffusive profiles for $\rho_{\text{core}} = 0$ as compared to the case of $\rho_{\text{core}} = 0.8$. Again for these results, the fully porous particles achieve better conversion and separation of components. The results so far are further confirmed by the results given in Table 3, showing the conversion rates for increasing values of ρ_{core} for non-isothermal condition ($\Delta H_A = -60 \text{ kJ/mol}$, $\Delta H_R = -20 \text{ kJ/mol}$). We see that increasing the core fraction radius, reduces the conversion rate of the reactant (component 1) to products (components 2 and 3). This is true because increasing ρ_{core} , reduces the binding capacity of the reactant and results in reduced conversion. Lastly, Figs. 12 and 13 give the results for the fully nonlinear isotherm case. Here, the behavior of the well-known nonlinear Langmuir isotherm, which displays peak tailings in the profiles, is evident. Despite the fluctuations of the temperature profiles, the conversion of the reactant to products for $\rho_{\text{core}} = 0.8$ (Fig. 13) is less again, as compared to that of fully porous particles case (Fig. 12).

TABLE 1. Parameters for test problems

Description	Symbols	Value	Unit
Bed void volume fraction	ϵ_b	0.4	—
Particle porosity	ϵ_p	0.333	—
Axial Peclet numbers	$Pe_{z,i}, Pe_{z,T}$	1500	—
Radial Peclet numbers	$Pe_{\rho,i}, Pe_{\rho,T}$	37.5	—
Dimensionless constant	η_i	2.7	—
Dimensionless constant	η_T	0.7	—
Dimensionless constants	ζ_i, ζ_T	40	—
Adsorption constant for c_1	a_1	1.0	—
Adsorption constant for c_2	a_2	0.2	—
Adsorption constant for c_3	a_3	1.8	—
Interstitial velocity	u	62×10^{-4}	<i>m/min</i>
Column length	L	0.27	<i>m</i>
Injection time (dimensionless)	τ_{inj}	1.0	—
Injected concentration of c_1	$c_{b,1}^{inj}$	3.0	<i>mol/l</i>
Injected concentrations of c_2, c_3	$c_{b,2}^{inj}, c_{b,3}^{inj}$	0.0	<i>mol/l</i>
Reaction equilibrium constant	K_{eq}^{het}	2.0	<i>mol/l</i>
Heterogeneous reaction rate constant	k^{het}	6.0×10^{-3}	<i>min</i> ⁻¹
Reference temperature	T^{ref}	300	<i>K</i>
Activation energy	E_A^{het}	60	<i>kJ/mol</i>
General gas constant	R_g	0.008314	<i>kJ/molK</i>
Density times heat capacity in liquid phase	$\rho^L c_p^L$	4.0	<i>kJ/Kl</i>
Density times heat capacity in solid phase	$\rho^S c_p^S$	4.0	<i>kJ/Kl</i>

 TABLE 2. Here, $X_1[\%] = 100 \times ((n_1^{inj} - n_1^{out})/n_1^{inj})$

Parameters [<i>kJ/mol</i>]	$X_A[\%]$	$X_A[\%]$	$\Delta H_{err}[\text{kJ}]$	$E_H[\%]$
	($\rho_{core} = 0$)	($\rho_{core} = 0.8$)		
$\Delta H_A = 0, \Delta H_R = 0$	28	14	—	—
$\Delta H_A = 0, \Delta H_R = -20, E_A^{het} = 60$	31	15	0.09	0.91
$\Delta H_A = 0, \Delta H_R = -40, E_A^{het} = 60$	34	16	0.23	0.96
$\Delta H_A = -60, \Delta H_R = -20, E_A^{het} = 60$	28	14	0.003	0.03
$\Delta H_A = -60, \Delta H_R = -20, E_A^{het} = 100$	41	19	0.05	0.34

 TABLE 3. Effects of increasing ρ_{core}

ρ_{core}	$X_A[\%]$
0 (fully porous)	28
0.2	25
0.4	24
0.6	21
0.8	14
0.9 (thin shell)	9

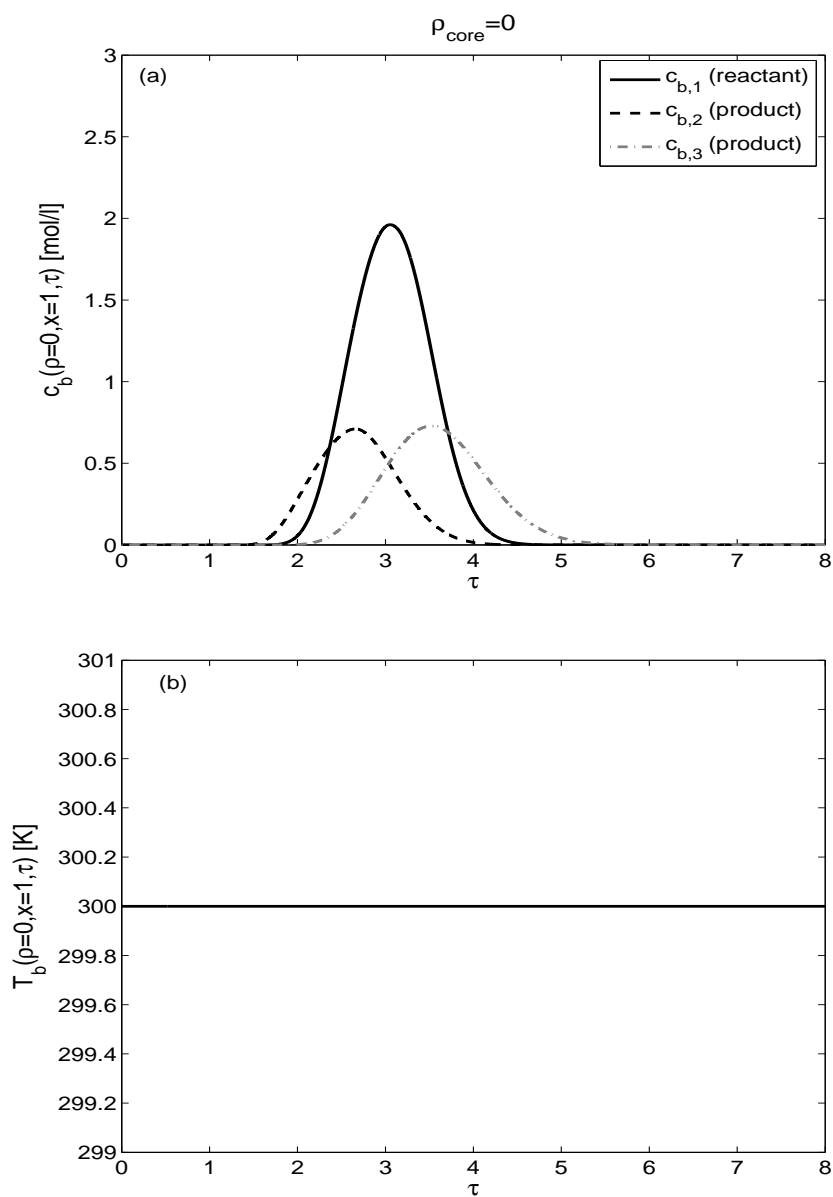


FIGURE 2. Isothermal Case: $\Delta H_A = 0 \text{ kJ/mol}$, $\Delta H_R = 0 \text{ kJ/mol}$, $b_j^{\text{ref}} = 0$ for $j = 1, 2, 3$.

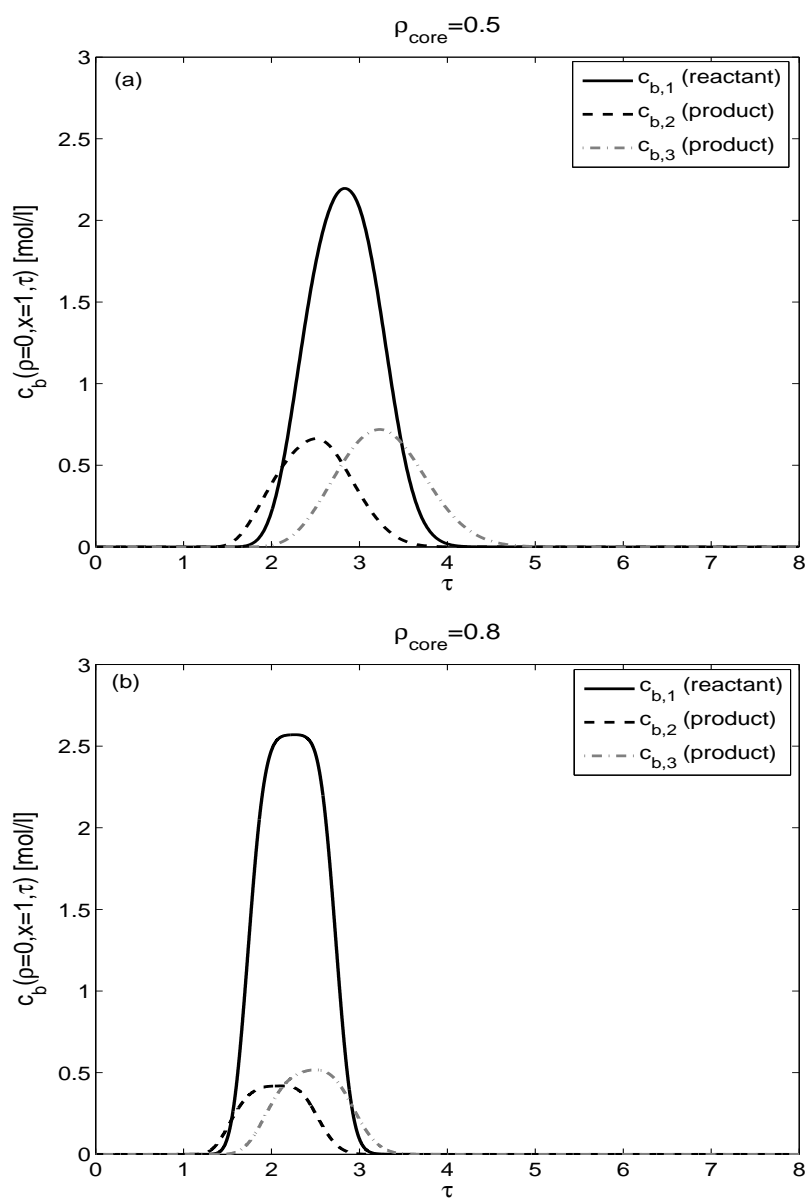


FIGURE 3. Isothermal Case: $\Delta H_A = 0 \text{ kJ/mol}$, $\Delta H_R = 0 \text{ kJ/mol}$, $b_j^{\text{ref}} = 0$ for $j = 1, 2, 3$.

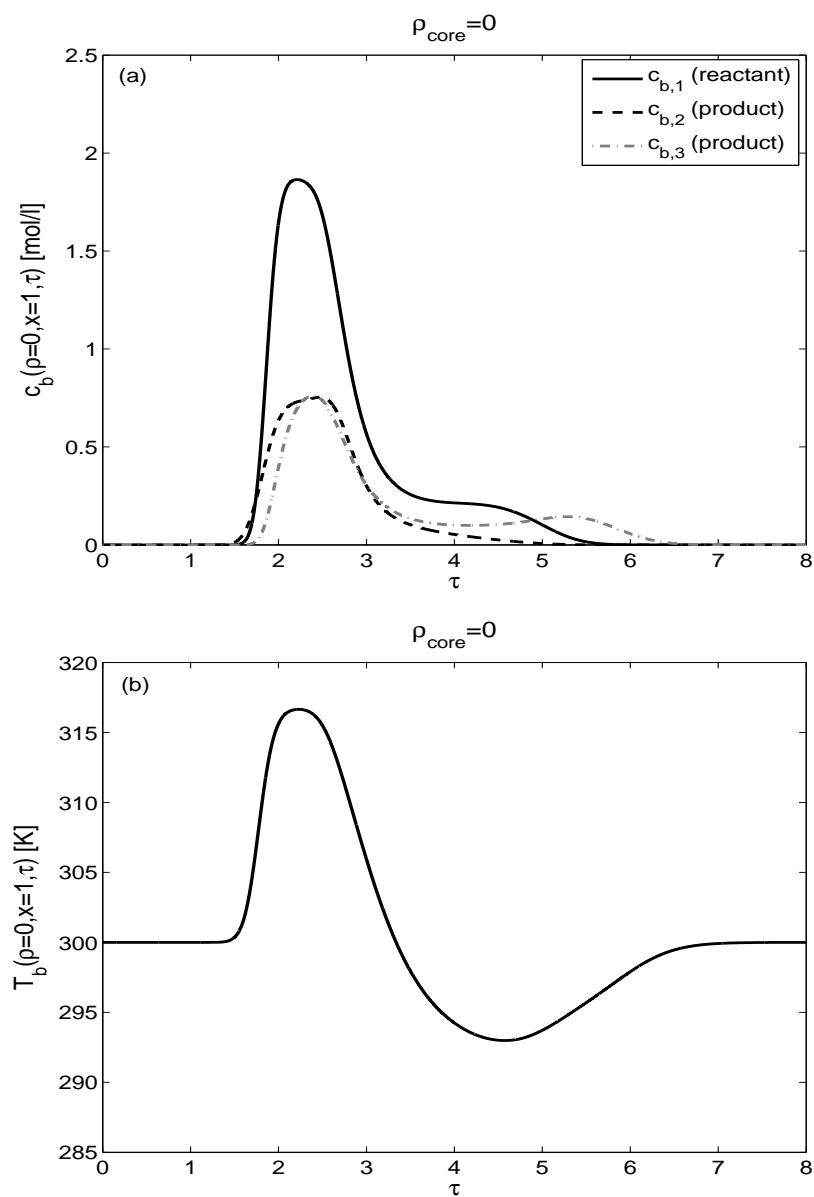


FIGURE 4. Non-isothermal Case: $\Delta H_A = -60 \text{ kJ/mol}$, $\Delta H_R = -20 \text{ kJ/mol}$, $b_j^{\text{ref}} = 0$ for $j = 1, 2, 3$.

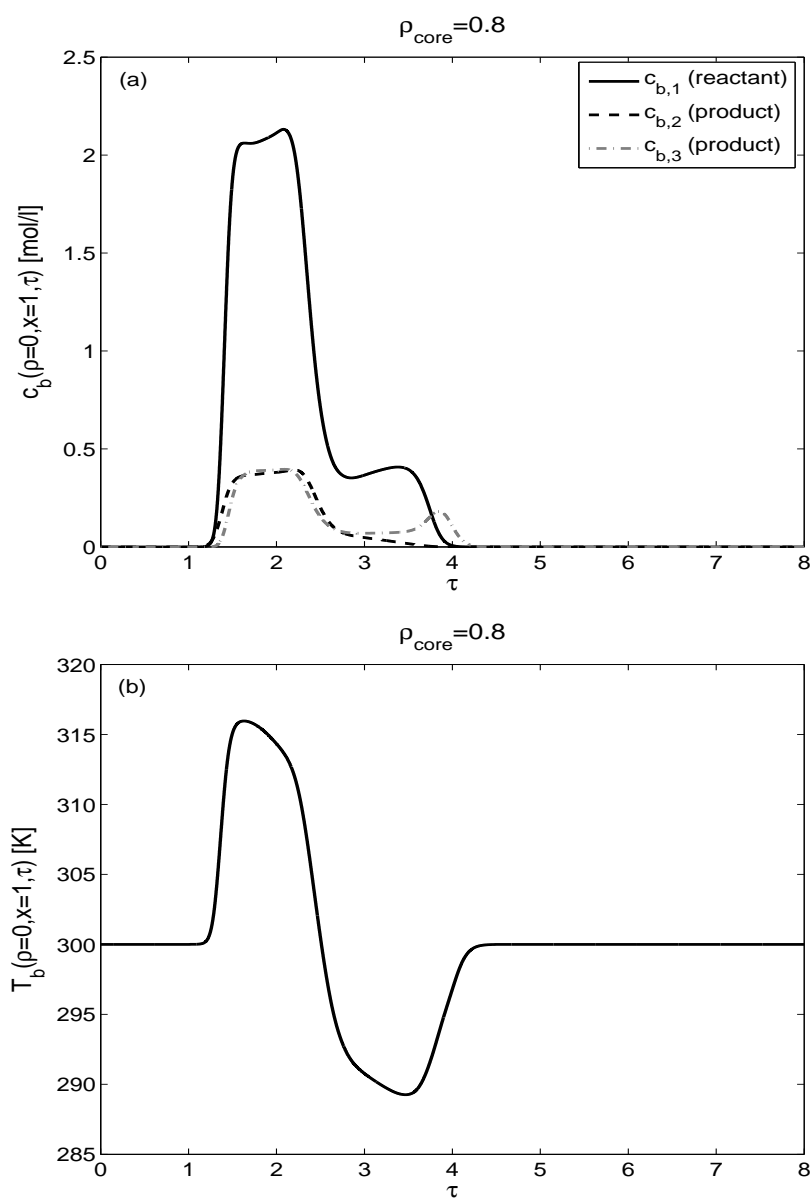


FIGURE 5. Non-isothermal Case: $\Delta H_A = -60 \text{ kJ/mol}$, $\Delta H_R = -20 \text{ kJ/mol}$, $b_j^{\text{ref}} = 0$ for $j = 1, 2, 3$.

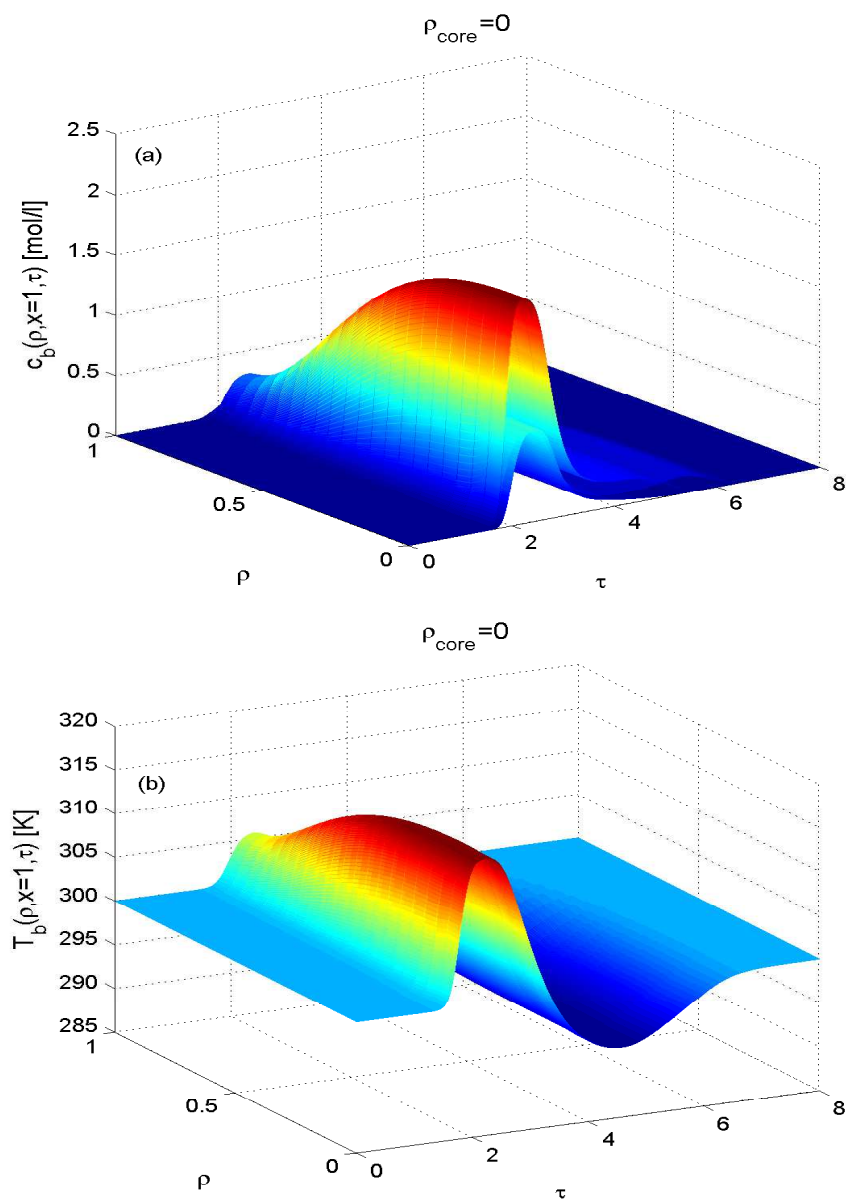


FIGURE 6. Non-isothermal Case: $\Delta H_A = -60 \text{ kJ/mol}$, $\Delta H_R = -20 \text{ kJ/mol}$, $b_j^{\text{ref}} = 0$ for $j = 1, 2, 3$.

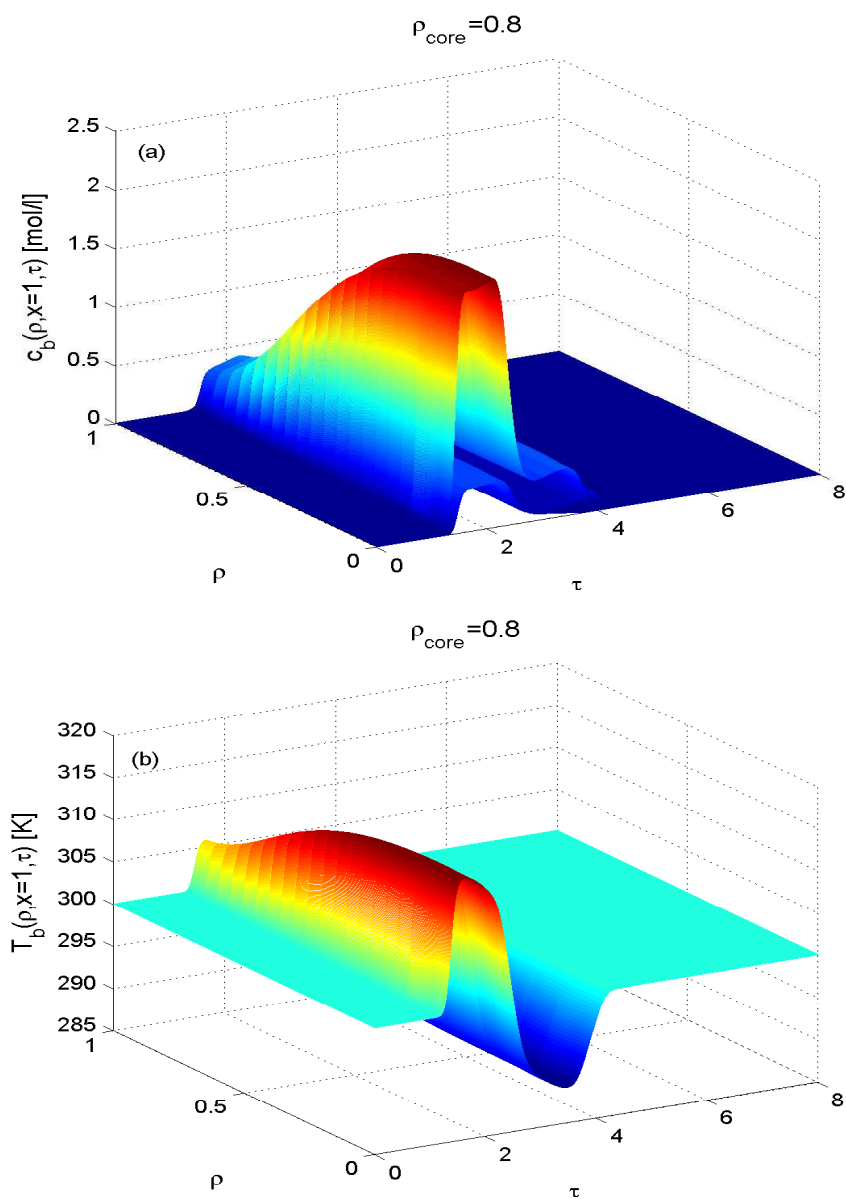


FIGURE 7. Non-isothermal Case: $\Delta H_A = -60 \text{ kJ/mol}$, $\Delta H_R = -20 \text{ kJ/mol}$, $b_j^{\text{ref}} = 0$ for $j = 1, 2, 3$.

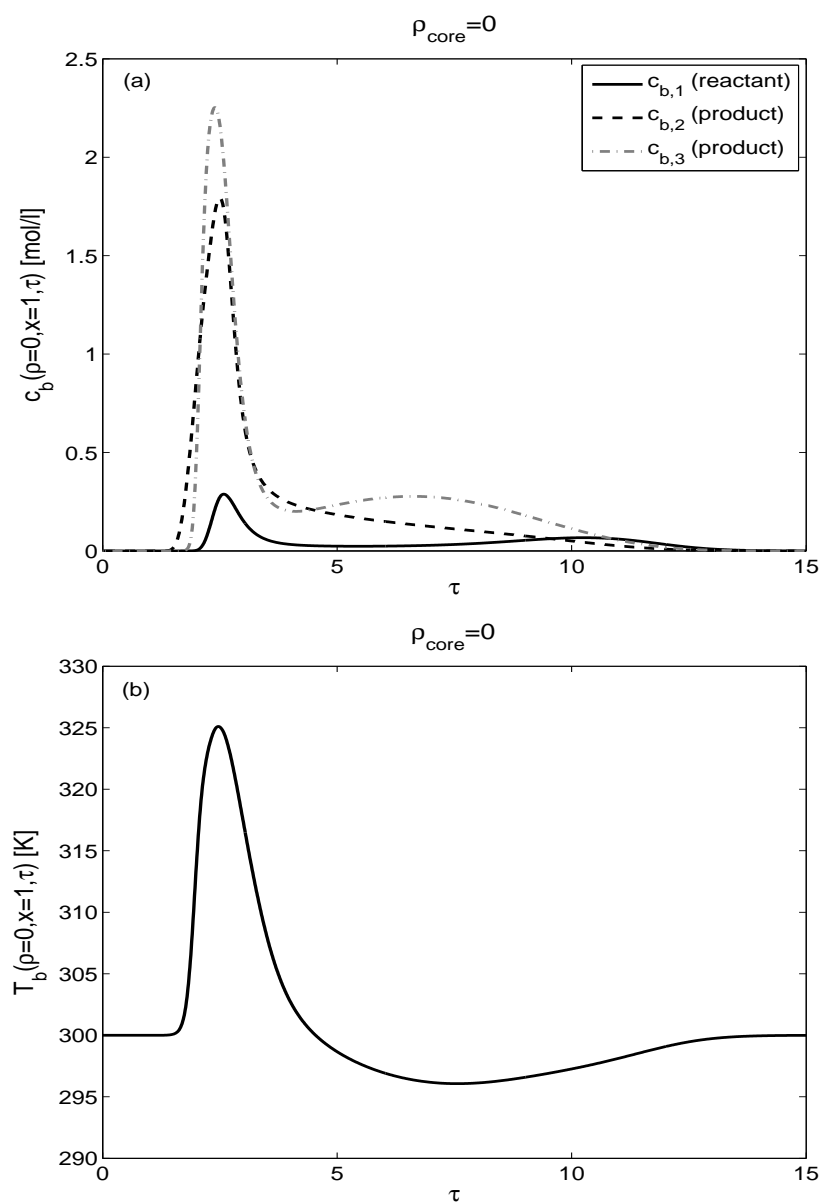


FIGURE 8. Non-isothermal Case: $a_1 = 6.0$, $a_2 = 0.2$, $a_3 = 2.0$, $\Delta H_A = -60 \text{ kJ/mol}$, $\Delta H_R = -20 \text{ kJ/mol}$, $b_j^{\text{ref}} = 0$ for $j = 1, 2, 3$.

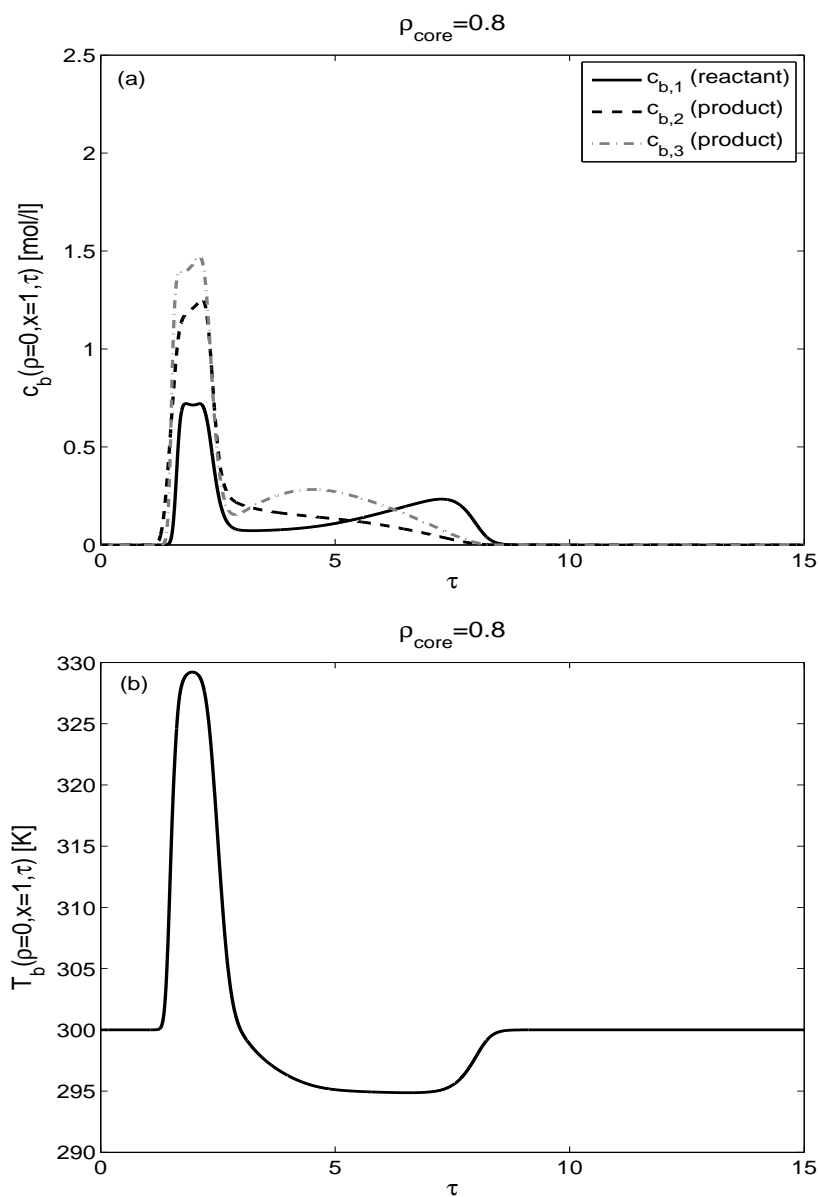


FIGURE 9. Non-isothermal Case: $a_1 = 6.0$, $a_2 = 0.2$, $a_3 = 2.0$, $\Delta H_A = -60 \text{ kJ/mol}$, $\Delta H_R = -20 \text{ kJ/mol}$, $b_j^{\text{ref}} = 0$ for $j = 1, 2, 3$.

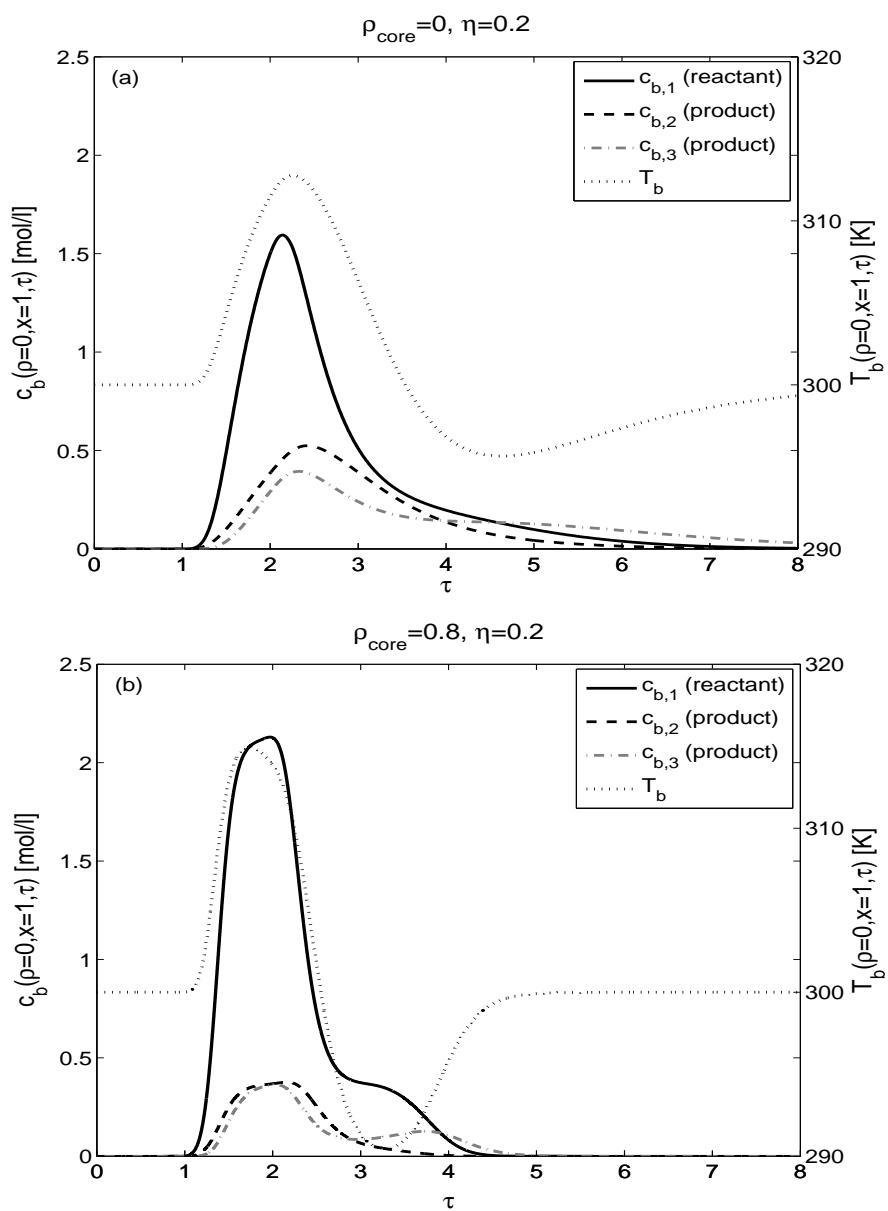


FIGURE 10. Non-isothermal Case: $\Delta H_A = -60 \text{ kJ/mol}$, $\Delta H_R = -20 \text{ kJ/mol}$, $b_j^{\text{ref}} = 0$ for $j = 1, 2, 3$.

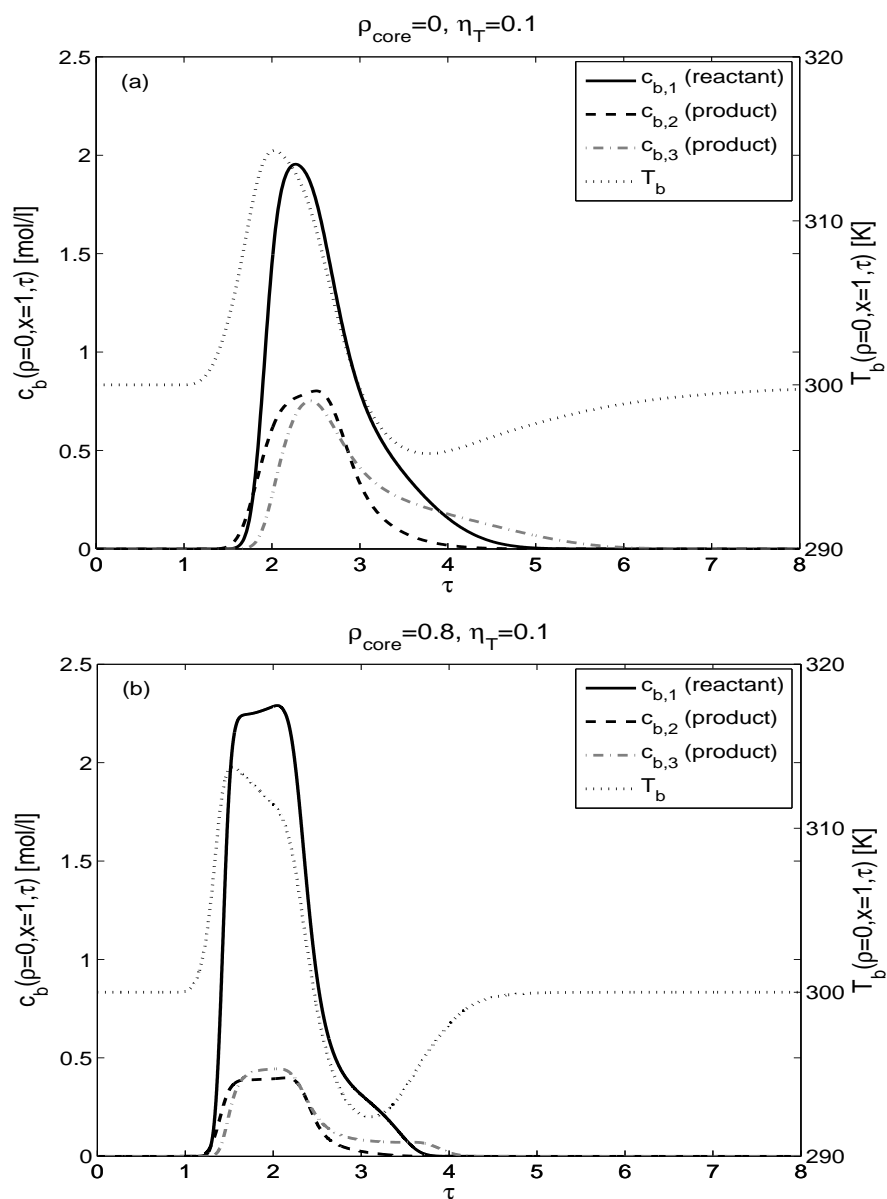


FIGURE 11. Non-isothermal Case: $\Delta H_A = -60 \text{ kJ/mol}$, $\Delta H_R = -20 \text{ kJ/mol}$, $b_j^{\text{ref}} = 0$ for $j = 1, 2, 3$.

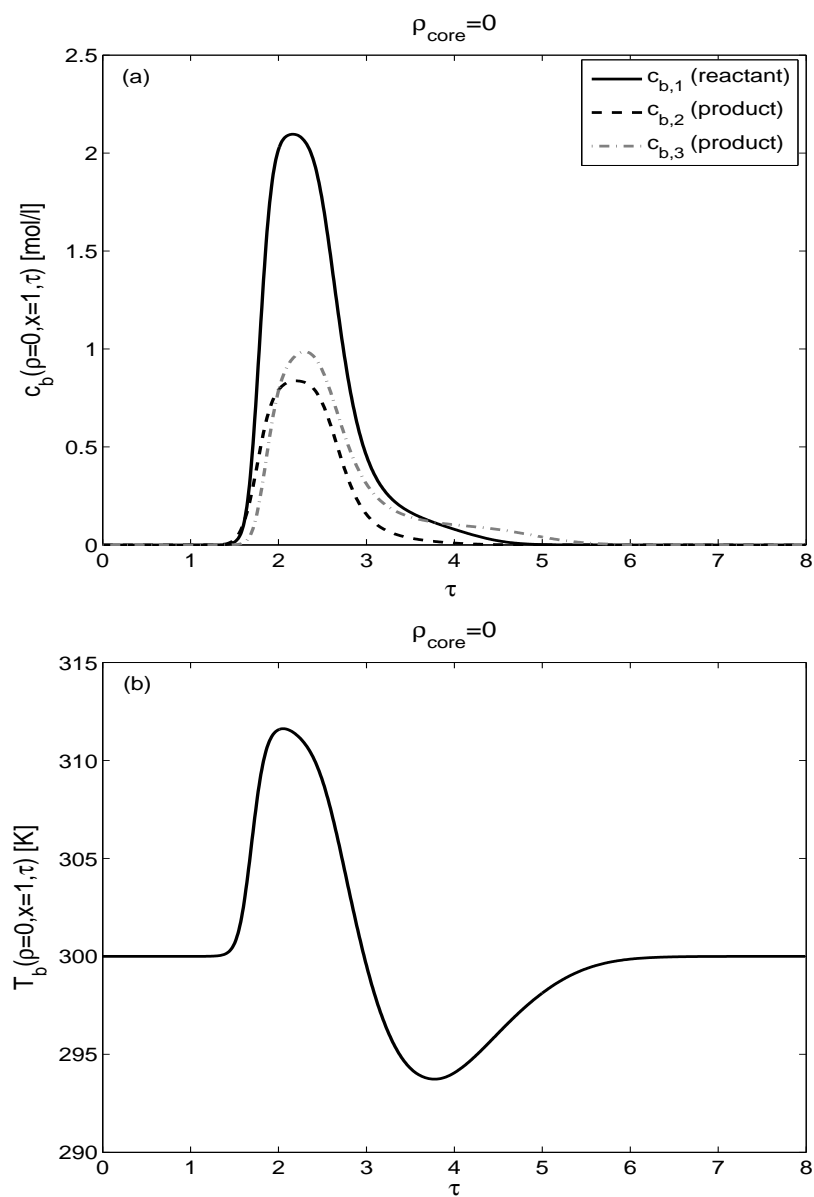


FIGURE 12. Non-isothermal Case: $\Delta H_A = -60 \text{ kJ/mol}$, $\Delta H_R = -20 \text{ kJ/mol}$, $b_j^{\text{ref}} = 1$ for $j = 1, 2, 3$.

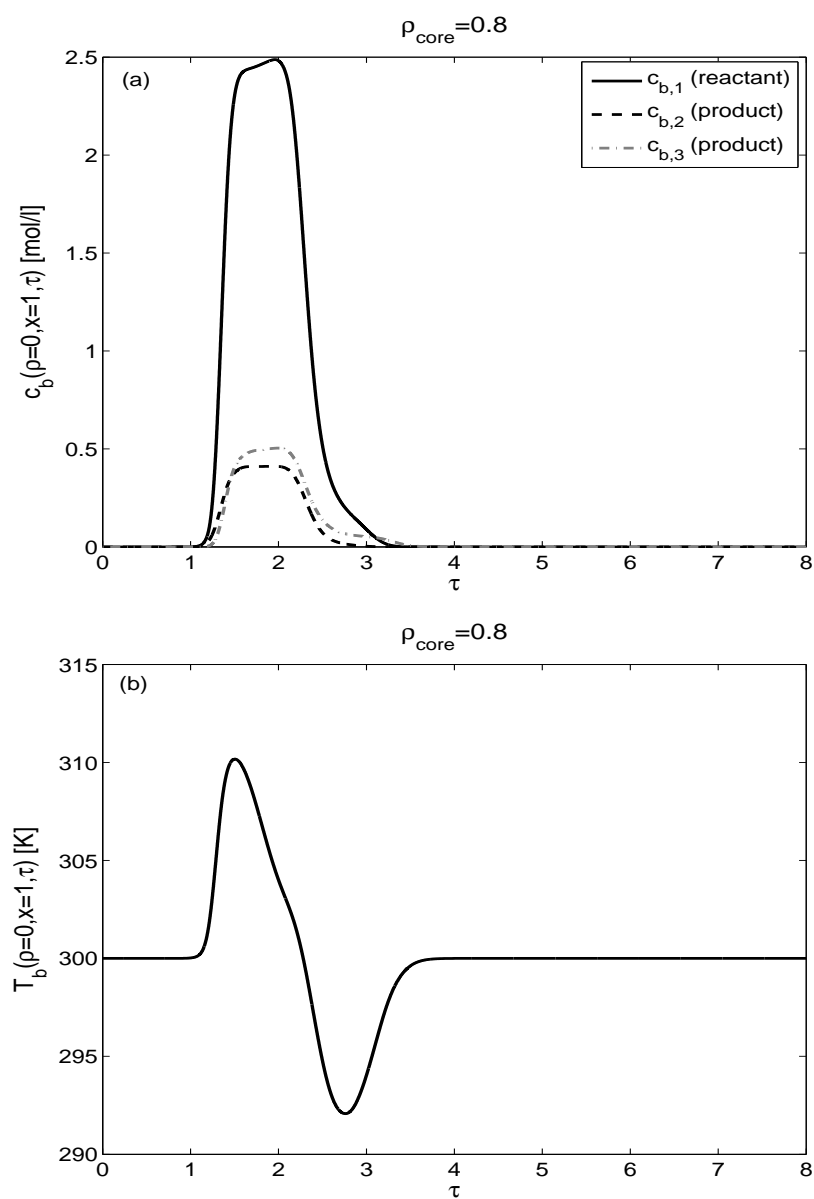


FIGURE 13. Non-isothermal Case: $\Delta H_A = -60 \text{ kJ/mol}$, $\Delta H_R = -20 \text{ kJ/mol}$, $b_j^{\text{ref}} = 1$ for $j = 1, 2, 3$.

6. CONCLUSION

The effects of core-shell particles on 2D non-isothermal reactive chromatography for conversion and separation of chemical components were investigated by formulating and implementing a two-dimensional general rate model of cylindrical geometry. The model is made up of a system of convection-diffusion-reaction partial differential equations. The formulated model is highly nonlinear and its solutions were numerically approximated by applying a high resolution finite volume scheme. The consistency of the results were validated and several test cases were carried out. The results show that the application of core-shell particles for separation and conversion in non-isothermal reactive chromatography, provides no advantage over the use of fully porous particles. Although they achieve sharper and narrower concentration profiles, increasing the value of the core radius fraction was found to cause reduction in the conversion rate of the reactant to products.

REFERENCES

- [1] G. Guiochon, *Preparative liquid chromatography*, J. Chromatogr. A **965** 129-161, 2002.
- [2] G. Guiochon, A. Felinger, D. G. Shirazi, A. M. Katti, *Fundamentals of preparative and nonlinear chromatography 2nd ed.* New York, Elsevier Academic press, 2006.
- [3] T. Borren, J. Fricke, *Chromatographic reactors in preparative chromatography of fine chemicals and pharmaceutical agents*, H. Schmidt-Traub (ed.) Wiley-VCH Verlag, Weinheim, 371-395, 2005.
- [4] J. J. Kirkland, F. A. Truszkowski, C. H. Dilks, G. S. Engel, *Superficially porous silica microspheres for fast high-performance liquid chromatography of macromolecules*, J. Chromatogr. A **890** 3-13, 2000.
- [5] S. Fekete, K. Ganzler, J. Fekete, *Facts and myths about columns packed with sub-3 μm and sub-2 μm particles*, J. Pharma. Biomed. Anal. **51** 56-64, 2010.
- [6] R. Rissler, *Separation of polyesters by gradient reversed-phase high-performance liquid chromatography on a 1.5 μm non-porous column*, J. Chromatogr. A **871** 243-258, 2000.
- [7] Y. Q. Xiang, B. W. Yan, C. V. McNeff, P. W. Carr, M. L. Lee, *Synthesis of micron diameter polybutadiene-encapsulated non-porous zirconia particles for ultrahigh pressure liquid chromatography*, J. Chromatogr. A **1002** 71-78, 2003.
- [8] K. Miyabe, *Evaluation of chromatographic performance of various packing materials having different structural characteristics as stationary phase for fast high performance liquid chromatography by new moment equations*, J. Chromatogr. A **1183** 49-64, 2008.

- [9] N. Manchon, M. D. Arrigo, A. Garcia-Lafuente, E. Guillamon, A. Villares, A. Ramos, J. A. Martinez, M. A. Rostagno, *Fast analysis of isoflavones by high-performance liquid chromatography using a column packed with fused-core particles*, *Talanta* **82** 1986-1994, 2010.
- [10] C. Wang, N. P. Soice, S. Ramaswamy, B. A. Gagnon, J. Umana, K. A. Cotoni, N. Bian, K. -S. C. Cheng, *Cored anion-exchange chromatography media for anti- body flow-through purification*, *J. Chromatogr. A* **1155** 74-84, 2007.
- [11] T. Gu, M. Liu, K. -S. C. Cheng, S. Ramaswamy, C. Wang, *A general rate model approach for the optimization of the core radius fraction for multi-component isocratic elution in preparative nonlinear liquid chromatography using cored beads*, *Chem. Eng. Sci.* **66** 3531-3539, 2011.
- [12] J. J. DeStefano, S. A. Schuster, J. M. Lawhorn, J. J. Kirkland, *Performance characteristics of new superficially porous particles*, *J. Chromatogr. A* **1258** 76-83, 2012.
- [13] L. E. Blue, J. W. Jorgenson, *1.1 μm superficially porous particles for liquid chromatography. Part I: Synthesis and particle structure characterization*, *J. Chromatogr. A* **1218** 7989-7995, 2011.
- [14] J. O. Omamogho, J. P. Hanrahan, J. Tobin, J. D. Glennon, *Structural variation of solid core and thickness of porous shell of 1.7 μm core-shell silica particles on chromatographic performance: Narrow bore columns*, *J. Chromatogr. A* **1218** 1942-1953, 2011.
- [15] G. Agrawal, J. Oh, B. Sreedhar, S. Tie, M. E. Donaldson, T. C. Frank, A. K. Schultz, A. S. Bommarius, Y. Kawajiri, *Optimization of reactive simulated moving bed systems with modulation of feed concentration for production of glycol ether ester*, *J. Chromatogr. A* **1360** 196-208, 2014.
- [16] S. Grüner, A. Kienle, *Equilibrium theory and nonlinear waves for reactive distillation columns and chromatographic reactors*, *Chem. Eng. Sci.* **59** 901-918, 2004.
- [17] G. Carta, *Exact analytical solution of a mathematical model for chromatographic operations*, *Chem. Eng. Sci.* **43** 2877-2883, 1988.
- [18] G. Guiochon, B. Lin, *Modeling for preparative chromatography*, Academic Press, 2003.
- [19] D. M. Ruthven, *Principles of adsorption and adsorption processes*, Wiley-Interscience, New York, 1984.
- [20] S. Qamar, U. D. Uche, F. U. Khan, A. Seidel-Morgenstern, *Analysis of linear two-dimensional general rate model for chromatographic columns of cylindrical geometry*, *J. Chromatogr. A* **1496** 92-104, 2017.
- [21] U. D. Uche, S. Qamar, A. Seidel-Morgenstern, *Numerical approximation of a nonisothermal two-dimensional general rate model of reactive liquid chromatography*, *Int. J. Chem. Kinet.* **52** 134155, 2020. <https://doi.org/10.1002/kin.21337>
- [22] U. U. David, S. Qamar, A. Seidel-Morgenstern, *Analytical and numerical solutions of two-dimensional general rate models for liquid chromatographic columns packed with core-shell particles*, *Chem. Eng. Res. Design* **130** 295-320, 2018.

- [23] S. Javeed, S. Qamar, A. Seidel-Morgenstern, G. Warnecke, *Efficient and accurate numerical simulation of nonlinear chromatographic processes*, J. Comput. Chem. Eng. **35** 2294-2305, 2011.
- [24] E. V. Lieres, J. Andersson, *A fast and accurate solver for the general rate model of column liquid chromatography*. *Journal of Computers and Chemical Engineering*, **34** 11801191, 2010.
- [25] B. Koren, *A robust upwind discretization method for advection, diffusion and source terms*, In C. B. Vreugdenhil, B. Koren, editors, *Numerical Methods for Advection-Diffusion Problems*, Volume 45 of *Notes on Numerical Fluid Mechanics*, chapter 5, pages 117-138, Vieweg Verlag, Braunschweig, 1993.
- [26] B. Cockburn, C. -W. Shu, *TVB Runge-Kutta local projection discontinuous Galerkin finite element method for conservation laws II, Gerneral framework*, *Mathematics of Computation* **52** 411-435, 1989.
- [27] S. Javeed, S. Qamar, A. Seidel-Morgenstern, G. Warnecke, *Parametric study of thermal effects in reactive liquid chromatography*, *Chem. Eng. J.* **191** 426-440, 2012.
- [28] T. Sainio, M. Kaspereit, A. Kienle, A. Seidel-Morgenstern, *Thermal effects in reactive liquid chromatography*, *Chem. Eng. Sci.* **62** 5674-5681, 2007.
- [29] T.D. Vu, A. Seidel-Morgenstern, *Quantifying temperature and flow rate effects on the performance of a fixed-bed chromatographic reactor*, *J. Chromatogr. A* **1218** 8097-8109, 2011.

DEPARTMENT OF MATHEMATICS PROGRAMME, NATIONAL MATHEMATICAL CENTRE ABUJA, NIGERIA

E-mail address: duj_uche@yahoo.com

DEPARTMENT OF MATHEMATICS PROGRAMME, NATIONAL MATHEMATICAL CENTRE ABUJA, NIGERIA

E-mail address: longsmarcy@yahoo.com

DEPARTMENT OF MATHEMATICS PROGRAMME, NATIONAL MATHEMATICAL CENTRE ABUJA, NIGERIA

E-mail address: folayanfe@gmail.com